Ultralong-range energy transport in a disordered organic semiconductor at room temperature via coherent exciton-polariton propagation

Shaocong Hou, Mandeep Khatoniar, Kan Ding, Yue Qu, Alexander Napolov, Vinod M. Menon, Stephen R. Forrest*

S.C. Hou, Y. Qu, A. Napolov, Prof. S.R. Forrest

Department of Electrical Engineering and Computer Science, University of Michigan, Ann Arbor, Michigan 48109, USA
E-mail: stevefor@umich.edu

M. Khatoniar, Prof. V.M. Menon
Department of Physics, City College of New York, City University of New York, USA

K. Ding, Prof. S.R. Forrest

Department of Physics, University of Michigan, Ann Arbor, Michigan 48109, USA

Prof. S.R. Forrest

Department of Materials Science and Engineering, University of Michigan, Ann Arbor, Michigan 48109, USA

Amorphous molecular solids are inherently disordered, exhibiting undesirable property of strong exciton localization for high-performance photonic and optoelectronics applications. Optical microcavities containing such disordered excitonic materials have been theoretically shown to support both propagating and localized exciton-polariton modes. In this work, the ultrastrong coupling of a Bloch surface wave photon and molecular excitons in a disordered organic thin-film at room temperature is demonstrated, where the major fraction of the polaritons are propagating states. The delocalized exciton-polariton has a group velocity as high as 3×10^7 m/s and a lifetime of 500 fs, leading to propagation distances of over one hundred microns from the excitation source. The polariton intensity shows a halo-like pattern that is due to self-interference of the polariton mode, from which we derive a coherence length of 20 μm and correlate it with phase-breaking of polariton scattering. Our demonstration of ultralong-range exciton-polariton transport at room temperature promises new photonic and optoelectronic applications such as efficient energy transfer in disordered condensed matter systems.

Long range excited state energy transport is a fundamental process in natural photosynthesis. As such, it can be exploited in numerous optoelectronic applications, such as organic photovoltaics and light-emitting devices.[1,2] In a molecular system, the excitation energy is localized in Frenkel excitons with large binding energies, and their transport occurs by near-field Förster or Dexter intermolecular hopping that is severely limited by a combination of the intrinsic dynamic disorder as well as considerable static disorder in amorphous films. Incoherent transport and strong localization typically lead to short exciton diffusion lengths < 10 nm, and diffusion constants of <10^{-3} cm^2/s. As a result, many efforts have been made to reduce material disorder, such as precise tailoring of molecular structure and the growth of ordered assemblies. Unfortunately, this has met with only limited success, resulting in exciton transport over only a micron or less.[3–5]

Compared with excitons, long range photon propagation has only limited interactions with the solid. Thus, a promising means to improve energy transport is to strongly couple excitons with photons in an optical cavity, forming new quantum mechanical quasi-particles called exciton-polaritons.[6–10] Polaritons partially inherit the light effective mass and delocalization properties rendered by their photonic component, and thus are potentially immune from interactions with local defects and disorder common to molecular solids.[11–13] Coherent coupling with an extended and propagating photon mode can lead to rapid and long-range transport that differs from the slow and short-range diffusion of more massive excitons. [14–16] However, it is still a challenge to experimentally visualize polariton transport, as it is essential to simultaneously confirm the presence of two anti-crossing lower and upper polariton branches, and a larger Rabi splitting than energy broadening of the exciton or cavity photon alone. Furthermore, it is important to exclude contributions from other weakly-coupled propagating photon modes. According to these criteria, room temperature polariton transport was recently observed over a few microns in a metal clad organic microcavity via ultrafast microscopy.[17] This distance, however, is almost one order of

magnitude smaller than that typically observed for inorganic crystalline cavity polaritons at cryogenic temperatures.[7]

In this work, we investigate room temperature polariton propagation in an all-dielectric photonic structure comprising a disordered molecular thin-film of tetraphenyldibenzoperiflanthene (DBP), a model organic electronic molecule, deposited onto the surface of a distributed Bragg reflector (DBR). Similar to the surface confined and propagating modes of one-dimensional or two-dimensional photonic crystals,[18,19] the truncated periodic multilayers of DBR support a Bloch surface mode, of which its strong electric-field enhancement and low optical loss is ideal for strong coupling with excitons and long-range transport applications.[20,21] Angular reflectivity measurements show two anti-crossing polariton branches with a giant vacuum Rabi splitting energy of 480 meV due to ultrastrong coupling between 0-0 vibronic of the molecular excitons and Bloch surface modes. Using spatial and momentum-resolved photoluminescence imaging measurements, we observe polariton transport over distances of at least 100 μm, and a halo-like intensity pattern due to polariton self-interference. Our model of polariton transport indicates that the hole size is determined by the coherence length correlated to phase-breaking by inelastic scattering, while the total propagation distance depends on the attenuation coefficient that includes material absorption and other scattering processes.

The sample consists of a DBR comprising 4 pairs of ZnS/MgF_2 followed by a 20 nm-thick DBP film on a fused silica substrate. The DBR supports a single transverse-electric (TE) Bloch surface wave (BSW) above the total internal reflection (TIR) angle ($\vartheta_{TIR} = 42^{\circ}$). The DBP film is amorphous with a low surface roughness (see AFM data and X-ray diffraction in Figure S1 and Figure S2, respectively). It exhibits three distinct vibronics (0-0, 0-1, 0-2) of its lowest spin-singlet exciton, corresponding to three absorption peaks (610 nm, 560 nm and 520 nm) and Stokes-shifted emission peaks (615 nm, 670 nm and 730 nm) in **Figure 1**a, right. The simulated TE angular reflectivity spectrum of the

structure using transfer matrix formalism is shown in Figure 1a, left. In the spectrum, two kinds of modes are distinguished: one comprises weakly-coupled parabolic modes at the upper edge of the DBR upper stopband (USB) extending to both below and above the TIR angle, and the other is bended near DBP excitonic energy due to the anti-crossing polariton modes (upper polariton branch: UP, lower polariton branch: LP) at $\theta > \theta_{TIR}$. All TE modes are directly visualized by the room temperature, white-light angular reflectivity measurement shown in Figure 1a, middle. Specifically, the reflectivity dip of the LP is sharp and faint, indicating the high-quality factor of the coupled BSW. The dip of the UP appears above the 0-2 transition, and narrows when approaching higher in-plane momentum, $n_0\sin\theta$, that is found at higher angles. (Here, n_0 is the glass index of refraction.) The presence of the two polariton branches provides clear evidence of strong coupling between photons and excitons, which is absent in previous reports on polariton propagation.[14,15,22]

We measured the room temperature TE angular photoluminescence emission spectrum of an encapsulated sample using a *k*-space microscope (see Experimental Section). As shown in Figure 1b, there is significant leakage of exciton emission from the USB at $\theta < \theta_{TIR}$ due to the limited spectral range of the DBR stop band. At $\theta > \theta_{TIR}$, only the lowest polariton branch LP is observed, and the maximum intensity is close to the emission peak of the 0-2 vibronic (Figure 1a, right), indicating phonon-assisted polariton relaxation.[16]

To track the polariton propagation, we image the spatial distribution of photoluminescence via non-resonantly exciting the sample with a tightly focused laser beam using the setup in the transmission configuration, and the pumping light cannot be coupled into any surface modes of sample due to energy and momentum mismatch (see Figure S3). The photoluminescence image is now dominated by an intense and bright exciton emission at the excitation spot due to the Gaussian spatial profile of the 1 µm diameter laser beam. Outside of this bright spot, relatively weaker emission radially spreads beyond the field of view. To rule out this weakly-coupled exciton emission

leakage from the USB, we place a slit filter in the reconstructed in-plane momentum k-space behind the imaging collection lens in the detection channel, and select only the high-k polariton emission at $\theta > \theta_{TIR}$ (see the relative position of the slit filter and k-space in Figure S4). The polariton emission propagating in the direction selected by the slit is shown in **Figure 2**a. Surprisingly, the polariton emission intensity is weak near the excitation spot, has a peak at a distance of approximately 20-30 µm, and then exponentially decays along the propagating path beyond the field of view that extends to 80 µm (see Figure 2b). For comparison, the emission profile taken in the absence of a k-space filter is also shown in Figure 2b, where a long and weak emission tail overlaps with the narrow and intense peak at the pumping position.

To verify whether the long-range propagation is due to polariton and not guided photons, we further select a portion of area at the intermediate image plane with a pinhole filter to probe the spectral dispersion as a function of position. When the pinhole coincides with the excitation spot corresponding to the observation distance of $L = 0$, a similar angular photoluminescence spectrum is obtained in **Figure 3**a, although the primary emission is from excitons in the USB rather than from LP. As the pinhole is moved away from the excitation spot along the propagation direction (increasing L), the weight of the polariton emission from LP increases, consistent with the propagation pattern observed in Figure 2. At $L = 17$ µm and beyond, the emission is dominated by the forward-propagating LP branch with a negative in-plane momentum shown in Figure 3b. Note that the pinhole filter causes considerable broadening of measured polariton modes, however, an energy blue shift of 10-15 meV is observed when polaritons propagate from the pumping center to $L = 17$ µm (see Figure S5), indicating thermal-assisted propagation at room temperature. In addition, much weaker emission from the LP branch corresponding to positive momentum is also observed. This suggests that during propagation, some polaritons back-scatter, and propagate in the opposite direction.

In a microcavity consisting of disordered materials, the incoherent exciton states can strongly interact with a photon, forming coherent polariton states that propagate like a plane wave. [13] However, the intrinsic structural and energetic disorders break the conservation of wave vector, leading to rapid decoherence of the excited states. The microscopic theory of conventional disordered microcavities[13,23] distinguishes four propagation regimes from zero to large k in the lower polariton branch: Anderson localization of polaritons, inelastic-scattering dominated polariton propagation, elastic-scattering dominated polariton propagation, and strong localization of weakly coupled exciton states. In BSW polaritons, the lower boundary of wavevectors is restricted by the total internal reflection angle, θ_{TIR}, and the polariton in the first localization regime is replaced by another weakly coupled exciton state. Thus, all BSW polaritons represent propagating modes.

After nonresonant excitation, photogenerated hot excitons rapidly relax to the exciton reservoir where they radiatively decay via weakly-coupled localized modes, such as leakage from the USB. At the same time, excitons in the reservoirs populate the LP polariton states via phonon-assisted recombination and/or radiative pumping.[16] As polaritons have large group velocities, they rapidly propagate in-plane, away from the pumping region. Thus, the lifetimes and group velocities of polaritons in the LP branch determine the spatial extent of the quasiparticle distribution.

To calculate the polariton lifetime, we fit the dispersion relation in Figure 1a with a coupled-oscillator model outside of the rotating-wave approximation[24,25] for three DBP vibronics, and one BSW photonic oscillator (see Experimental Section). Figure 1a (left) shows the four calculated branches (red dashed lines), where the UP and LP dispersions match the measured data, although absorption from the middle polariton (MP) branches is too weak to be observed.[25] The fitting yields a vacuum Rabi-splitting energy of 480±50 meV between the 0-0 exciton and the Bloch surface wave, which is significantly larger than the damping rates of uncoupled excitons and photons, confirming excitation in the strong coupling regime. Moreover, this giant splitting is > 20% of the uncoupled 0-0

exciton energy which nominally corresponds to ultrastrong cavity coupling.[24] This ultrastrong-coupled system shows a high excitonic fraction from 20% to 60% in the LP branch from lower to higher k. Considering the lifetimes and fractions of the uncoupled DBP singlet exciton and the BSW photon, the calculated polariton lifetime is 500 fs for the photonic-like LP, and 7 ps for the excitonic-like LP quasiparticles. We also obtained a group velocity in the LP branch of 0.5 - 3×10^7 m/s directly measured from the dispersion relation in Figure 1a.

To understand the polariton propagation pattern, we measured the wavelength-resolved polariton emission profiles in **Figure 4**a using the k-space filter. For each wavelength, the signal shows a similar halo-like pattern with the polariton emission maximum located tens of micrometers away from the excitation point, followed by decreasing intensity with distance. The size of the hole decreases with the wavelength (λ), with an approximate radius of 20 μm at a wavelength of λ = 670 nm and 10 μm at λ = 750 nm. We attribute the polariton propagation pattern to self-interference between two light paths illustrated in Figure 4b. The polariton mode is either directly excited by the radiation field of an exciton (path 1), or after experiencing TIR (path 2) from the DBP film surface. The phase difference between the two paths results in destructive interference at the pumping site. As the polariton mode propagates beyond the coherence length approximately corresponding to the radius of the halo, the emission intensity rapidly increases to a maximum, followed by an exponential decay due to scattering and non-negligible material absorption.

For simplicity, we take a pair of planewave components of the spherical dipole radiation field with the same in-plane momentum and calculate the polariton propagation pattern (see Experimental Section). In Figure 4c, we find that the calculation (solid lines) provides a fit to the halo-like profile observed in wavelength-resolved propagation measurement (data points). The size of the halo, L_{hole}, is determined by the coherence length, l_{coh} (see Experimental Section), of polariton propagation, which is limited by decoherence mechanisms including scatterings from grain

boundaries, surface roughness, and interaction among polaritons and phonons.[7,26,27] The hole diameter decreases with increasing wavelength as the polariton mode approaches the air cone at θ_{TIR}.

Note that we also observe a similar halo-like emission intensity pattern from the TM guided modes in the same sample (see Figure S6), and from the high-k substrate mode in the sample lacking a DBR (Figure S7), both of which are weakly coupled to the DBP exciton radiation field. This supports our model that the wave-like nature of photons and polaritons leads to the halo propagation patterns. [28]

Polariton propagation is affected by many interacting processes, such as elastic/inelastic scattering and nonlinear polariton interactions. Elastic/inelastic scattering processes are inevitable in organic polaritons due to intrinsic material disorder. Other processes such as interactions with phonons or photons escaping from the cavity,[13] contribute to inelastic scattering, and this is confirmed by the energetic blue shift during polariton propagation. We calculate the phase-breaking length, l_{inel}, for inelastic scattering with the group velocity and lifetime of the polariton following previous analyses.[13] The phase-breaking length is as long as 23 μm at short wavelengths (large k), and monotonically decreases to 18 μm at a longer wavelengths (smaller k). To gain further understanding of processes limiting the propagation distance, in Figure 4d we plot four characteristic lengths, that is, the coherence length l_{coh} and phase-breaking length l_{inel}, along with the hole size L_{hole}, and the total propagation length $L_{1/e}$ as obtained by fitting an exponential to the propagation pattern decay with distance. (see details in Experimental Section) Clearly, the phase-breaking length l_{inel} is close to the coherence length l_{coh}. We speculate that inelastic polariton scattering dominates their decoherence, and thus has a significant impact on hole size L_{hole} in the propagation pattern. In contrast, $L_{1/e}$ has a wavelength-dependence that differs substantially from the other three lengths. Beyond the halo, other loss processes come into play in attenuating polariton propagation. The

decrease in amplitude beyond the halo is ascribed to absorption and resonant scattering by the tail of the density of exciton states, which leads to an ultralong propagation length up to 120 µm.

We also observe a blueshift in the PL spectrum of up to 1 meV when the non-resonant pumping power increases from 0.2 µW to 2 mW. This nonlinear effect mainly comes from interactions of polariton with a large concentration of localized excitons generated at the reservoir near the pumping spot. However, this blue shift is one order of magnitude smaller than the energy broadening of the polariton modes (approximately 10 meV), and hence it is less likely to create an effective potential plateau that repels polariton from the pumping spot. Indeed, the polariton propagation pattern does not change with the pumping power, indicating the nonlinearity plays only a minor role in this case.

In conclusion, we have demonstrated exceptionally long range, room temperature transport of strongly coupled exciton-polaritons in a one-sided distributed Bragg reflector, which is orders of magnitude larger than expected for excitons in disordered organic semiconductors. The observed polariton intensity shows a halo-like pattern which is explained by the self-interference of polariton modes. Our work shows that to realize long range and efficient polariton transport in disordered systems, it is essential to eliminate the strongly localized polariton components, increase the coherence and phase-breaking lengths, as well as reduce other losses, such as absorption and scattering. Compared with short-range Förster and Dexter-mediated exciton diffusion, polaritons provide an alternative path to transport of excitation energy to a remote location. Furthermore, the simplicity of open dielectric optical structures enables a range of device architectures. For example, the robust nature of polaritons can reduce requirements for use of highly ordered solids, leading to, for example, efficient long-range energy harvesting in organic photovoltaics that mimic photosynthetic processes under ambient conditions, while also advancing our understanding of polariton physics.

9

Experimental Section

Device fabrication: The device was fabricated by sequentially depositing 4 pairs of a 90 nm thick ZnS and a 148 nm thick MgF$_2$ layer, then 20 nm-thick DBP layer on a 180 micrometer-thick fused silica substrate via thermal evaporation in a vacuum chamber with a base pressure of 10^{-7} torr, and encapsulated using a thin fused silica lid and ultraviolet cured epoxy in an ultrapure N$_2$ environment.

Material characterization: A 20 nm-thick DBP layer on a fused silica substrate was deposited with the same conditions used for XRD (Rigaku Ultima IV X-Ray Diffractometer) and AFM characterization (Bruker Dimension Icon, ScanAsyst mode).

Optical measurements: The angular reflectivity and photoluminescence spectra were measured using a k-space microscope comprising an inverted microscope with a 1.40 NA, 100X objective (Olympus), a white lamp source (for reflectivity), TM-polarized λ = 532 nm ultrafast pulsed laser source (Toptica Fibre-Pro, for PL), a k-space lens, a TE polarizer, a λ = 600 nm long pass filter (for PL), and a spectrometer (Acton SpectraPro SP-2500) with a 1024 x 1024 CCD camera (PIX 1024B, Princeton Instruments). The photoluminescence images were collected by the k-space microscope in a transmission geometry. A 1 μm diameter TM-polarized pulsed Gaussian laser beam was focused on the surface of the DBP layer with a 0.5NA, 50X objective from the DBP side, and the emission was collected with another 1.40 NA, 100X objective from the substrate side. Before projecting it to the spectrometer or camera, delay lenses were used to reconstruct k-space and real-space, where a slit filter in k-space or a pinhole filter in real-space was placed as designed. Details of the setup can be found in Supporting Information.

Simulations: Angular reflectivity of the sample was simulated using the transfer matrix method. The propagation pattern of polariton was calculated by a self-interference model, and details of calculation can be found in Supporting Information.

Supporting Information

Supporting Information is available from the Wiley Online Library or from the author.

Received: ((will be filled in by the editorial staff))
Revised: ((will be filled in by the editorial staff))
Published online: ((will be filled in by the editorial staff))

References

[1]   G. D. Scholes, G. R. Fleming, A. Olaya-Castro, R. Van Grondelle, *Nat. Chem.* **2011**, *3*, 763.

[2]   J. L. Brédas, E. H. Sargent, G. D. Scholes, *Nat. Mater.* **2016**, *16*, 35.

[3]   X. H. Jin, M. B. Price, J. R. Finnegan, C. E. Boott, J. M. Richter, A. Rao, S. Matthew Menke, R. H. Friend, G. R. Whittell, I. Manners, *Science* **2018**, *360*, 897.

[4]   A. T. Haedler, K. Kreger, A. Issac, B. Wittmann, M. Kivala, N. Hammer, J. Köhler, H. W. Schmidt, R. Hildner, *Nature* **2015**, *523*, 196.

[5]   H. Najafov, B. Lee, Q. Zhou, L. C. Feldman, V. Podzorov, *Nat. Mater.* **2010**, *9*, 938.

[6]   J. Schachenmayer, C. Genes, E. Tignone, G. Pupillo, *Phys. Rev. Lett.* **2015**, *114*, 196403.

[7]   D. M. Myers, S. Mukherjee, J. Beaumariage, D. W. Snoke, M. Steger, L. N. Pfeiffer, K. West, *Phys. Rev. B* **2018**, *98*, 235302.

[8]   S. K. Saikin, M. A. Shakirov, C. Kreisbeck, U. Peskin, Y. N. Proshin, A. Aspuru-Guzik, *J. Phys. Chem. C* **2017**, *121*, 24994.

[9]   S. K. Saikin, A. Eisfeld, S. Valleau, A. Aspuru-Guzik, *Nanophotonics* **2013**, *2*, 21.

[10]   J. Feist, F. J. Garcia-Vidal, *Phys. Rev. Lett.* **2015**, *114*, 196402.

[11]   V. M. Agranovich, M. Litinskaia, D. G. Lidzey, *Phys. Rev. B* **2003**, *67*, 085311.

[12]   P. Michetti, G. C. La Rocca, *Phys. Rev. B* **2005**, *71*, 115320.

[13]   M. Litinskaya, *Phys. Lett. A* **2008**, *372*, 3898.

[14]   G. Lerario, D. Ballarini, A. Fieramosca, A. Cannavale, A. Genco, F. Mangione, S. Gambino, L.

Dominici, M. De Giorgi, G. Gigli, D. Sanvitto, *Light Sci. Appl.* **2017**, *6*, e16212.

[15]   R. Pandya, R. Chen, Q. Gu, J. Sung, C. Schnedermann, O. S. Ojambati, R. Chikkaraddy, J. Gorman, G. Jacucci, O. D. Onelli, others, *arXiv Prepr.* **2019,** *arXiv1909.03220*.

[16]   D. M. Coles, P. Michetti, C. Clark, W. C. Tsoi, A. M. Adawi, J. S. Kim, D. G. Lidzey, *Adv. Funct. Mater.* **2011**, *21*, 3691.

[17]   G. G. Rozenman, K. Akulov, A. Golombek, T. Schwartz, *ACS Photonics* **2018**, *5, 105.*

[18]   P. Yeh, A. Yariv, C.-S. Hong, *J. Opt. Soc. Am.* **1977**, *67*, 423.

[19]   P. Halevi, *Phys. Rev. B* **1999**, *59*, 15112.

[20]   M. Liscidini, D. Gerace, D. Sanvitto, D. Bajoni, *Appl. Phys. Lett.* **2011**, *98*, 121118.

[21]   F. Barachati, A. Fieramosca, S. Hafezian, J. Gu, B. Chakraborty, D. Ballarini, L. Martinu, V. Menon, D. Sanvitto, S. Kéna-Cohen, *Nat. Nanotechnol.* **2018**, *13*, 906.

[22]   K. Takazawa, J. I. Inoue, K. Mitsuishi, T. Takamasu, *Phys. Rev. Lett.* **2010**, *105*, 067401.

[23]   M. Litinskaya, P. Reineker, *Phys. Rev. B* **2006**, *74,* 165320.

[24]   A. F. Kockum, A. Miranowicz, S. De Liberato, S. Savasta, F. Nori, *Nat. Rev. Phys.* **2019**, *1*, 19.

[25]   S. Hou, Y. Qu, X. Liu, S. R. Forrest, *Phys. Rev. B* **2019**, *100*, 045410.

[26]   S. Aberra Guebrou, C. Symonds, E. Homeyer, J. C. Plenet, Y. N. Gartstein, V. M. Agranovich, J. Bellessa, *Phys. Rev. Lett.* **2012**, *108*, 066401.

[27]   K. S. Daskalakis, S. A. Maier, S. Kéna-Cohen, *Phys. Rev. Lett.* **2015**, *115*, 035301.

[28]   D. G. Suárez-Forero, V. Ardizzone, S. F. da Silva, M. Reindl, A. Fieramosca, L. Polimeno, M. de Giorgi, L. Dominici, L. N. Pfeiffer, G. Gigli, others, *arXiv Prepr.* **2019**, *arXiv1908.03472*.
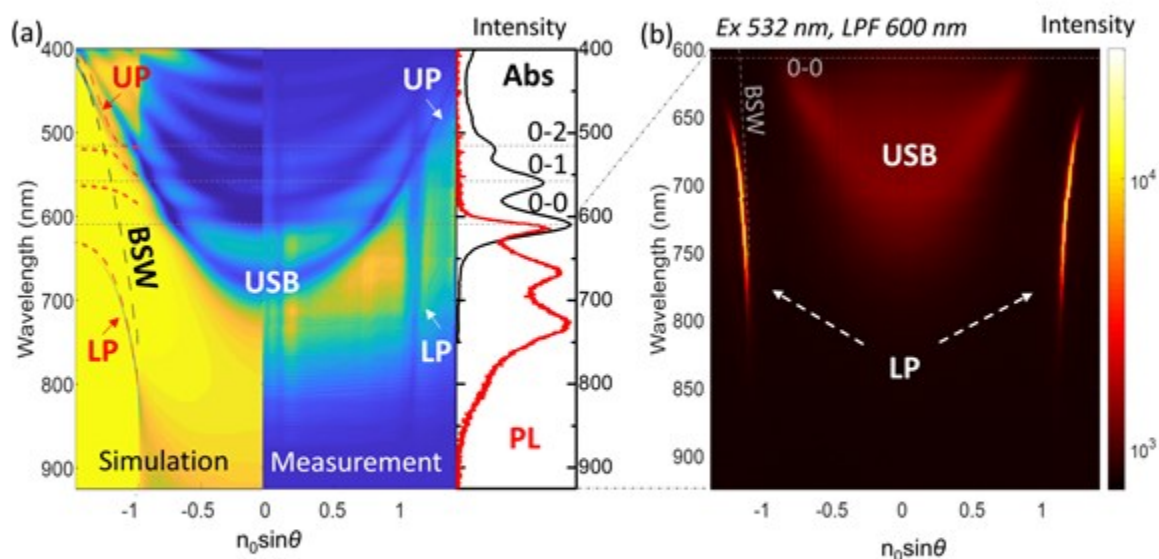
Figure 1. Ultrastrong coupling between DBP and Bloch surface waves (BSW). (a) Simulated (left) and measured (middle) transverse electric (TE) angular reflectivity spectra of ultrastrong coupled vibronic excitons of DBP (horizontal gray dashed-lines) and the BSW (black dashed-line). Red dashed lines show four fit polariton branches (UP: upper polariton branch, LP: lower polariton branch) using the coupled-oscillator model. Two vertical blue lines in the middle are artificial due to the setup. Absorption and photoluminescence spectra (right) of uncoupled DBP shows the vibronic progressions; (b) Measured TE angular photoluminescence spectra of the ultrastrong coupled sample using an laser excitation wavelength (Ex) at 532 nm and a long-pass spectral filter (LPF) cutting off at 600 nm. Gray dashed-lines show the uncoupled 0-0 exciton of DBP and the BSW.
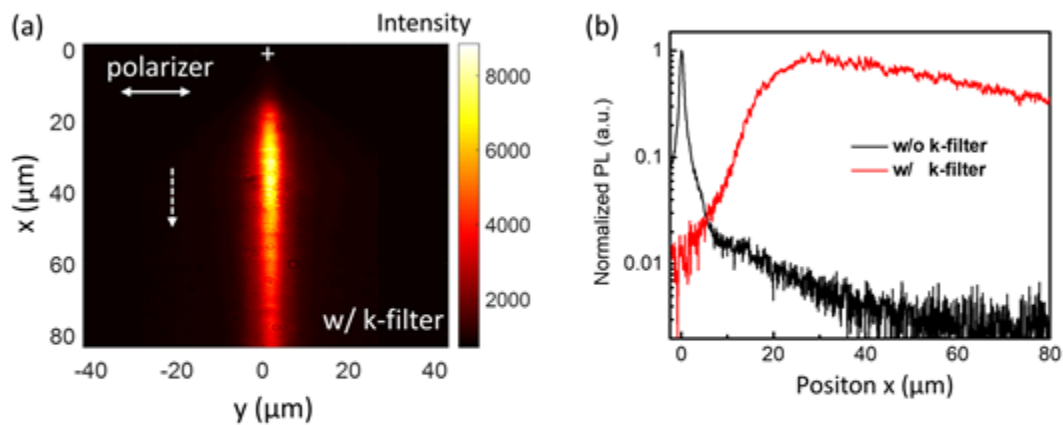
Figure 2. k-filtered photoluminescence imaging showing polariton propagation. (a) Real-space photoluminescence (PL) image using a k-space filter. The excitation laser spot is located at (0, 0), indicated by "+". The dashed arrow indicates the propagation direction. (b) PL emission intensity distribution along the propagation direction with (red) and without (black) a k-space filter.
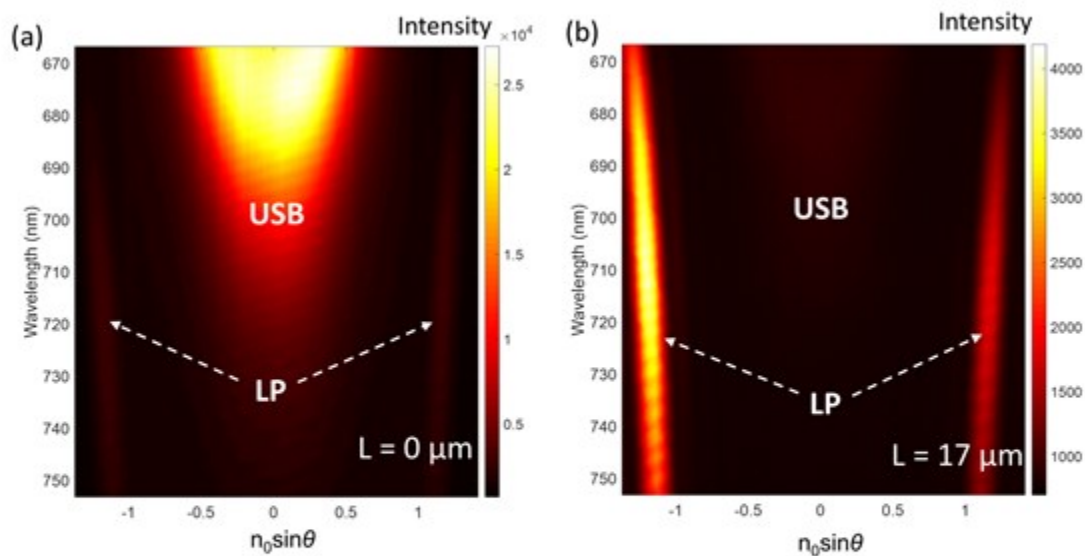
Figure 3. Selected-area angular PL spectra showing the origin of the emission. (a) k-space filtered PL dispersion of selected area at the position (a) L = 0 μm and (b) L = 17 μm from the laser excitation spot.
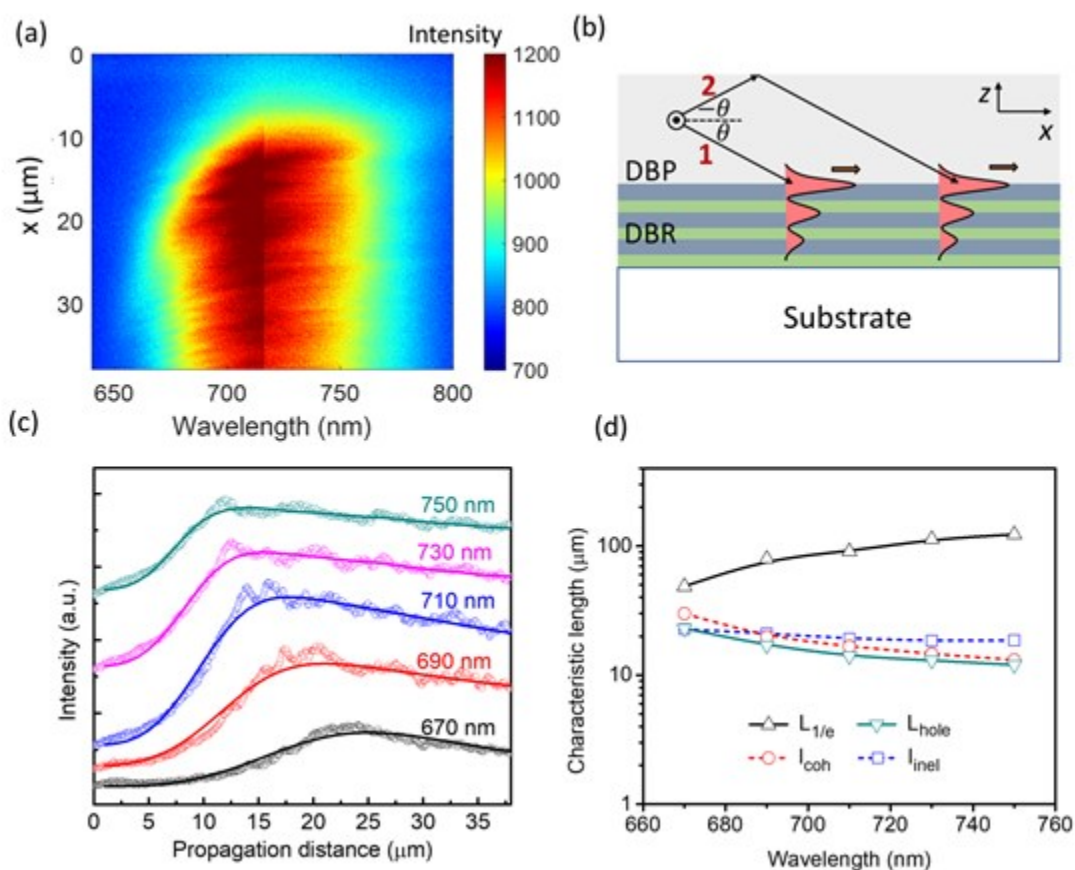
Figure 4. Polariton propagation experiment and model. (a) Energy-resolved propagation image. The vertical break at 720 nm results from combining two images collected in two sequential wavelength ranges. (b) The scheme shows the polariton self-interference model used to fit the propagation profiles in (a). (c) Five propagation profiles at wavelengths of 670, 690, 710, 730 and 750 nm. The calculated distributions (solid lines) are fit to the measured data (circular dots). (d) Comparison of the coherence length, l_{coh}, phase-breaking length, l_{inel}, the hole size, L_{hole} and the total propagation length $L_{1/e}$ vs, wavelength.

Long range excitation energy transport over 100 microns is demonstrated in an amorphous organic thin film on a DBR. The exciton exhibits ultrastrong coupling with a Bloch surface wave photon, overcoming short exciton diffusion lengths of disordered material systems. The halo-like polariton propagation pattern is explained by self-interference.

Keywords: energy transport, ultrastrong coupling, exciton-polariton, disordered materials, organic semiconductors

Shaocong Hou, Mandeep Khatoniar, Kan Ding, Yue Qu, Alexander Napolov, Vinod M. Menon, Stephen R. Forrest*

Ultralong-range energy transport in disordered organic semiconductors at room temperature via coherent exciton-polariton propagation